Applied and Computational Mechanics 16 (2022) 101–118

Fracture behavior of prestressed ductile target subjected to high velocity impact – Numerical study

Y. Jasra[a], R. K. Saxena[a,*]

[a] *Department of Mechanical Engineering, Sant Longowal Institute of Engineering and Technology, Deemed-to-be-University, Sangrur, Punjab, India*

Received 7 September 2022; accepted 21December 2022

Abstract

Impact studies are performed to evaluate the ballistic performance of material subjected to a high strain rate. At high velocities, the projectile penetrates through the material which leads to a fracture of the target body. The fracture behavior depends upon the condition of the target body. It is anticipated that the fracture behavior should depend upon the prestress condition of the target. Considering the aforementioned concern, the thermo-elastic-plastic finite element model is formulated using MSC Marc Mentat^{TM} to analyze the effect of the prestress condition of the target body on fracture behavior. A detailed comparison has been presented considering four different prestress states subjected to impact by a blunt-shaped projectile. The continuum damage mechanics using a stress triaxiality-based damage model is used to simulate damage evolution and fracture. It is found that the presence of prestress alters the overall fracture response of the structure subjected to high strain rate deformation. In the presence of tensile prestress, the material resists the accumulation of damage which is due to the lower values of stress triaxiality and equivalent plastic strain. It is also found that the presence of tensile prestress inside the target body increases the ballistic performance, whereas the presence of compressive prestress inside the target body degrades the performance.

Keywords: finite element analysis, prestress, mild steel, damage mechanics, high velocity impact

1. Introduction

The protection of engineering structures, vehicles and space shuttles against high velocity moving projectiles is gaining attention significantly due to the development of high-speed moving vehicles and advanced high-energy weapons. A high velocity moving projectile is an increasing threat to manned vehicles and structures each year. Due to the complex nature of the fracture of these structures, the impact phenomenon is still not fully intercepted and understood. Thus, there is a need for engineering structures to be designed and manufactured to withstand high velocity impacts. The interaction during the impact between the two bodies and the perforation in the target leads to catastrophic failure. The stress wave which initiates from the point of impact travels throughout the impacting bodies and leads to the overall fracture of the structure. The fracture in the ductile material evolves from the nucleation and coalescence of micro-voids that originate from the point of contact. It propagates throughout the material due to the viscous and localized plasticity and leads to catastrophic failure. The literature review reveals that several studies have been carried out related to the fracture of metallic target bodies in the form of a flat plate. Some of the relevant references related to fracture behavior in target bodies have been reported. Børvik et al. [3] analyzed the scanning electron microscope images of a perforated

*Corresponding author. Tel.: +91 921 622 00 06, e-mail: rksaxena04@yahoo.com.
https://doi.org/10.24132/acm.2022.779

Nomenclature			
σ	Cauchy stress	T	temperature
ε	Green-Lagrange strain	T_r	reference temperature
σ_{eq}	equivalent stress	T_m	melting temperature
ε^p_{eq}	equivalent plastic strain	R	external force
$\dot{\varepsilon}$	plastic strain rate	E	Young's modulus
$\dot{\varepsilon}_0$	reference strain rate	ν	Poisson's ratio
ε_f	fracture strain	ϱ	density
σ_m	mean stress	c_p	specific heat
u	displacement	t	time
V	volume	D	accumulated damage
$CorrI$	correlation index	D_c	critical value of damage

target body and found that the void nucleation is the initial phase proceeded by their growing and coalescing in the zones under compression. Børvik et al. [2, 4] analyzed the ballistic performance of 12 mm thick steel plates. It was reported that the ballistic performance of blunt projectiles increases when fired at low velocity as compared to the hemispherical projectile. Further, the performance of hemispherical and conical projectiles increases with the increase in velocity.

Teng et al. [21] evaluated six different fracture models to predict the fracture in Weldox 460 E steel and 2024-T351 aluminum plates subject to blunt and hemispherical projectiles. The scope of application for each model was discussed. The effect of fracture models on the fracture behavior in thin beams was evaluated. It was reported that the thin beams failed by shear plugging at a high velocity and by tensile tearing at a velocity near the ballistic limit[1]. Gupta et al. [9] evaluated the ballistic performance of a 1 mm thick aluminum plate. The effect of nose shape on the deformation of the plate using adaptive meshing was studied. The study related to the element size and the effect on the numerical prediction was reported. It is reported that the preloading on the target plate affects its response to fracture without affecting the ballistic limit [10]. Iqbal et al. [12] studied the characterization and prediction of fracture in 12 and 18 mm thick mild steel plates. The plates were impacted by 7.62 AP projectiles at varying incident angles. The incident angle was varied until the rebounding of the projectile. Mohammad et al. [16] analyzed the effect of the projectile nose on the perforation behavior of the target plates. In the study, multiple factors, i.e., projectile shape, impact angle, target thicknesses, and other variables, were varied to present an in-depth understanding of the fracture behavior. They found that the ballistic limit increases with increasing the angle of obliquity. The projectile shape is the prominent factor in the evaluation of fracture behavior and the ballistic limit increases in the case of hemispherical, conical and spherical shapes, but reduces for the blunt shape projectile. Gürgen and Kuşhan [11] investigated the effect of carbide additives in shear-thickening fluids. These fluids are extensively used in protective applications. It was found that the reinforcement with the carbide additives provides additional strength at low velocity. Domun et al. [6] investigated the fracture behavior of the nanomodified glass fiber-reinforced polymer by reinforcing the matrix with graphene and a modified version of the carbon nanotube to enhance the impact performance. They observed around a 16% increase in the ballistic limit for the modified

[1]The ballistic limit is the velocity required for a particular projectile to reliably (at least 50 % of the time) penetrate the target plate [5].

matrix. Researchers have applied different strategies to enhance the impact performance and investigated different parameters to have an in-depth understanding of the impact behavior. The impact phenomenon is so dynamic that by varying a single parameter, the fracture patterns and the overall failure behavior change.

Large ductile structures are typically built and assembled by combining smaller components and sections. The assembly of the required intended structures is accomplished by joining the various components using various fabrication methods. Welding is one of the most well-known and adaptable joining processes, with applications in nearly every type of service condition. Welding heat induces localized expansion, which is absorbed by the molten metal or the placement of the welded components during the welding process. Due to temperature gradients in the weldment, there is uneven contraction over the domain in both the longitudinal and transverse directions during welding, resulting in the generation of residual stress. Residual stress in the material ranges from tensile to compressive and is distributed unevenly throughout the joined components [14]. The type and magnitude of residual stress in the weldment have a significant impact on the fracture behavior of the structure. Further, different metal forming and processing operations may also induce residual stress. The presence of residual stress inside the material affects the response of the structure. Additionally, it is known that in-service components may experience residual stress due to different onsite processing and joining methods. Such residual stress may affect the impact behavior, especially the fracture. These residual stresses may operate as prestress.

The literature reveals that most of the studies focus on the fracture behavior of the material subject to high velocity impact and compared with the experimental observations. Numerous studies that depict the ballistic behavior of metallic plates impacted at high velocities may be found in the literature. To interpret the overall fracture behavior of the impacting plates, many parameters have been investigated such as projectile shapes, projectile velocities, target thicknesses and other variables. In order to represent the complicated fracture phenomenon, various modeling approaches are offered in the literature, but neither the role of prestress, which is generated during the fabrication process and contributes to the performance deterioration that occurs during in-service use nor an explicit comparison between stress-free and prestressed materials seem to have been addressed. Prestressed material may have a significant role during high velocity impact. It can either be detrimental or beneficial depending upon the application. Therefore, it is important to comprehend the function of prestress in the ductile target material and whether it affects the many conspicuous values, which eventually affect the fracture behavior. The present study analyzes and compares the fracture behavior for stress-free and prestressed target material under high velocity impact.

There is always a chance of high velocity impact on ships, underground prestressed pipelines and other structures. Thus, a deep understanding of the role of prestress during the impact has a lot of significance in multiple fields of application. Such a study finds its application for protective metallic sheets on armor vehicles and large pipes carrying high-pressure liquids. As a result, the focus of this research is to figure out what influence the prestress conditions contribute to the fracture behavior of a structure under high velocity impact.

Generally, processing and joining processes induce non-homogeneous prestress. To make the analysis simpler and to comprehend their role, uniform tensile and compressive prestresses have been considered. The objective of the present work is to simulate the process of deformation and to analyze the influence of tensile or compressive stress on the overall fracture behavior in a three-dimensional multi-axial prestressed material under high velocity impact. The continuum damage mechanics (CDM) model is employed to demonstrate fracture behav-

ior. The contribution of the present work is to provide an understanding of the possible fracture behavior of the ductile target material with the prestress condition under high velocity impact.

2. Materials and model

2.1. Finite element procedures used

For the mechanical analysis, finite element (FE) equations are developed using the concept of virtual work. After incorporating the body forces, the expression becomes [1]

$$\int_V \sigma_{ij}\,\delta(\Delta\varepsilon_{ij})\,\mathrm{d}V + \int_V \varrho\,\ddot{u}_i\,\delta(\Delta u_i)\,\mathrm{d}V = R, \tag{1}$$

where σ_{ij} is the Cauchy stress tensor, $\Delta\varepsilon_{ij}$ is the incremental Green-Lagrange strain tensor, $\delta(\Delta u_i)$ is the virtual incremental displacement vector, ϱ is the density of the material, $\ddot{u}_i$ is the acceleration, R is the incremental virtual work due to external forces and V is the volume. The usual summation rules apply for spatial coordinates x_i with $i = 1, 2, 3$. As the impact problem is a highly non-linear problem, to optimize the numerical dissipation, the generalized-α dynamic operator within implicit time integration schemes is used to solve the time derivative integral that is conditionally stable and recommended to be used for large deformation high strain rate contact-impact problems [13]. Non-linear FE equations are solved iteratively using the updated Lagrange formulation.

The temperature rise in the impact problem is due to the incremental plastic strain and also at the contact surface of two bodies due to frictional contact [7]. The equation for the transient heat transfer analysis is given by

$$\frac{\partial}{\partial x_i}\left(k\frac{\partial T}{\partial x_i}\right) + \dot{q} - \varrho\,c_p\frac{\partial T}{\partial t} = 0, \tag{2}$$

where T is the temperature, t is the time, c_p is the specific heat, k is the thermal conductivity and $\dot{q}$ is the internal heat generation per unit volume per unit time. Due to the short duration, the complete impact phenomenon is assumed to be adiabatic. The source of heat generation is due to the plastic deformation of the target and projectile. The internal heat generated per unit volume per unit time at a point is

$$\dot{q} = \frac{\beta}{\Delta t}\int_V \sigma_{ij}\Delta\varepsilon_{ij}, \tag{3}$$

where β is the fraction of plastic work converted to heat and Δt is the time increment. The value of β is 0.9 [8]. The Newmark method is used to convert the transient equation into an algebraic finite element equation [1]. The material is assumed to be isotropic. Eight-noded elements with reduced integration and large strain formulation are used in the analysis [1].

2.2. Constitutive material modeling

The plastic behavior is modeled using the Johnson-Cook plasticity model. The yield stress is expressed as

$$\bar{\sigma} = \left[A + B\left(\varepsilon_{eq}^{p}\right)^{n}\right]\left[1 + C\ln\left(\frac{\dot{\varepsilon}}{\dot{\varepsilon}_0}\right)\right]\left(1 - T_e^{m}\right), \tag{4}$$

where ε_{eq}^{p} is the equivalent plastic strain, A, B, n, C and m are the material constants, $\dot{\varepsilon}$ is the current value of plastic strain rate, $\dot{\varepsilon}_0$ is the reference strain rate coefficient and $T_e = (T - T_r)/(T_m - T_r)$ is the effective temperature with T being the current value of temperature, T_r is the reference temperature and T_m is the melting temperature for the material [22]. The continuum damage mechanics (CDM) model is employed to demonstrate the fracture under the high velocity impact [7]. In this model, the behavior of a material is described by introducing an additional scalar variable called the "damage". The accumulation of damage demonstrates void nucleation, void propagation and coalescence [15]. The accumulated damage at the integration point in a finite element is defined as [21]

$$D = \int_0^{\varepsilon^p} \frac{\mathrm{d}\varepsilon_{eq}^{p}}{\varepsilon_f}, \tag{5}$$

where $\mathrm{d}\varepsilon_{eq}^{p}$ is the increment in the equivalent plastic strain and ε_f is the fracture strain given by

$$\varepsilon_f = \left[D_1 + D_2 \exp\left(D_3 \frac{\sigma_m}{\sigma_{eq}}\right)\right]\left[1 + D_4 \ln\left(\frac{\dot{\varepsilon}}{\dot{\varepsilon}_0}\right)\right](1 + D_5 T_e^m), \tag{6}$$

where σ_m is the mean stress and σ_{eq} is the equivalent von Mises stress. The experimental data required to estimate the parameters for the fracture strain with respect to stress triaxiality, plastic strain rate and temperature, are derived from experimental and numerical studies on the tensile test [22]. The values for the D_1, D_2 and D_3 are $0.312\,5$, 0.935 and -1.25, respectively. The value for the D_4 is $-0.025\,4$ and D_5 is $0.526\,2$. The integration in (5) is performed on all integration points in an element. When the value of accumulated damage D exceeds the critical value of damage D_c at the integration point of an element, the element is subjected to be failed. The failed element loses stiffness and is completely removed from the target body.

2.3. Finite element models

The formulation is applied to simulate the fracture behavior of the plate subject to high velocity impact. The finite element analysis is performed using MSC Marc Mentat™. It is further added that the damage model, stiffness reduction factors and prestress conditions are incorporated as an external Fortran subroutine. The constitutive matrix of the material for each finite element is updated due to the accumulation of damage to model the element erosion. The element deletion is modeled using the "element birth and death" technique. The "element death" is assumed when the accumulated damage exceeds D_c during the impact. The effect of negative stress triaxiality termed "cut-off stress triaxiality" has been incorporated, i.e., the accumulation of damage in the given increment is not evaluated if the stress triaxiality is below $-1/3$ in a particular increment [18]. The two-body interaction involves the contact between adjoining surfaces. The "node-to-segment" contact algorithm is implemented for such interaction. The iterative penetration algorithm is applied to avoid penetration during the high velocity impact.

The FE formulation for thermo-mechanical analysis for the ballistic performance is validated using the work of Gupta et al. [9]. Subsequently, the formulation is applied to analyze the effect of prestress conditions on the fracture behavior for a flat target under high velocity impact. It is assumed that the target material is subjected to prior tensile or compressive load giving rise to entrapped prestress of tensile and compressive nature, respectively. The load is released just before the impact to find the effect of these prestress conditions on fracture behavior under high velocity impact. Four different cases are analyzed for fracture behavior. Initially,

the stress-free target is impacted by a blunt-shaped projectile. In view of the earlier study [14] regarding the residual stress formation in a weldment, the target is assumed to have a prestress of 280 MPa. The validated model is applied to study the effect of prestress on the fracture behavior of the target body in the form of a flat square plate under impact with a blunt projectile. The finite element model for the problem is kept the same as given in Fig. 1. The finite element mesh is given in Fig. 2. The mesh density is kept higher under the impact zone to capture the gradients in the response variables. The mesh density is coarser away from the impact zone to optimize the number of elements. The mesh in the x–y plane is kept the same for validation with an element length of 0.4 mm for high mesh density and 6 mm for coarse mesh density, totaling 6 084 eight-noded hexahedral reduced integration elements in the x–y plane. A total of 20 elements along the thickness direction are taken for 6 mm plate thickness. The material for the target body is mild steel and its properties are presented in Table 1. The thickness of the target body is 6 mm. The dimensions for the target plate are given in Fig. 1. The target plate is assumed to be fixed at the outer edges. The dimensions for the target plate (280 mm $\times$ 280 mm) are intentionally taken much larger than the projectile diameter (19 mm) to minimize the effect of end constraints on the fracture behavior under high velocity impact. The projectile has an initial velocity of 400 m s^{-1}. The effect is analyzed on fracture behavior, stress triaxiality, equivalent plastic strain, accumulation of damage and von Mises stress.

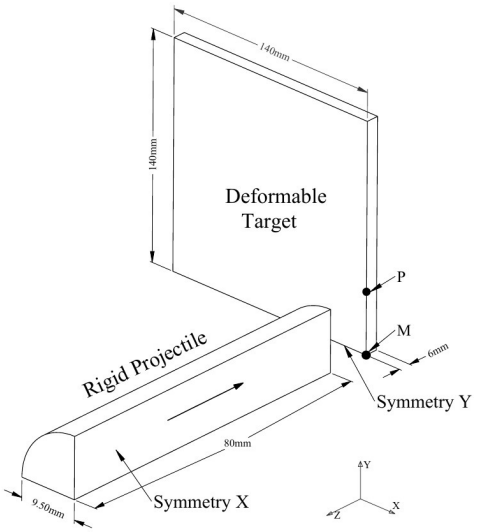

Fig. 1. Schematic of the impact problem

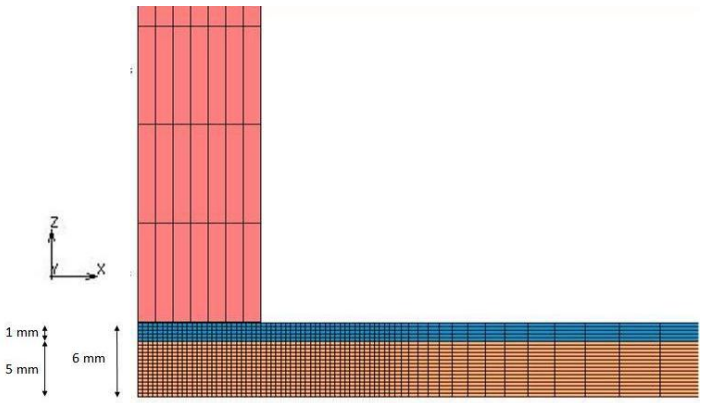

Fig. 2. Finite element mesh of the impact problem

In the first case, a uniform tensile prestress of 280 MPa is assumed. Later, the target is assumed to have a uniform compressive prestress of 280 MPa and at the last, the target is subjected to the combined tensile and compressive prestress of 280 MPa. The prestress conditions in the target material are imposed at the Gauss points as an initial condition. The fundamental adequacy of the model is not compromised by including the initial conditions in (1) as evidenced by Bathe [1]. Saleh et al. [20] have also applied a similar approach to incorporate the residual stress along the rolling direction and transverse direction due to metal forming operation. These initial conditions are imposed using external Fortran subroutines. As stated earlier, the uniform prestress conditions are applied considering the one-quarter domain to simplify the analysis and to get an understanding. The analysis with full domain in addition to non-homogeneous prestress conditions will be performed in the extension of the present work.

Tab. 1. Material properties for mild steel [22]

Property	Value
Modulus of elasticity, E	203 GPa
Poisson's ratio, ν	0.3
Density, ϱ	7 850 kg m^{-3}
Initial yield stress, A	363 MPa
Hardening modulus, B	792.71 MPa
Hardening exponent, n	0.575 6
Strain rate coefficient, C	0.000 54
Reference strain rate, $\dot{\varepsilon}_0$	0.000 5
Temperature exponent, m	1.64
Melting temperature, T_m	1 798 K
Reference temperature, T_r	298 K
Specific heat, c_p	400 J kg^{-1}K^{-1}
Critical value of damage, D_c	0.9

3. Results and discussion

3.1. FE model validation

A coupled thermo-mechanical finite element formulation is applied to simulate the impact of a rigid blunt-shaped projectile on the deformable flat target. The schematic of the problem is given in Fig. 1 and the finite element mesh is shown in Fig. 2. For the validation, a total of 48 672 hexahedral reduced integration elements are used for the 1 mm thick target plate. In view of the available literature, there is no such study that has analyzed the effect of prestress on the fracture behavior of the material under high velocity impact. Accordingly, validation of the model is performed for the non-prestress state. The formulation is validated by the experimental results from Gupta et al. [9]. The material properties, geometric dimensions of the problem and the damage model for validation are referenced by Gupta et al. [9]. The simulations for validation purposes are performed with five different velocities: 73.9, 87.5, 92.5, 102.5, and 115.6 m s^{-1}. The validation results, in terms of residual velocity of the projectile at different velocities and deflection of the target body at 115.6 m s^{-1}, are given in Fig. 3. It is observed that the results are in good agreement with the experimental findings of Gupta et al. [9]. Small deviations are observed in the results, which may be due to the material and mathematical approximations in the finite element formulations. To assess the validated results and to quantify the deviation of predicted values from the experimental results, the correlation index is defined as [17]

$$CorrI = 1 - \sqrt{\frac{\sum d_i^2}{\sum E_i^2}}, \tag{7}$$

where d_i represents the difference between the predicted and experimental values and E_i represents the respective experimental value. The unity value for the correlation index reflects the perfect match. For the present work, $CorrI = 0.974$ for the residual velocity and $CorrI = 0.964$ for the deflection of the target plate. The $CorrI$ values show that the residual velocity of the projectile and deflection of the target plate exhibits good agreement with the experimental observations.

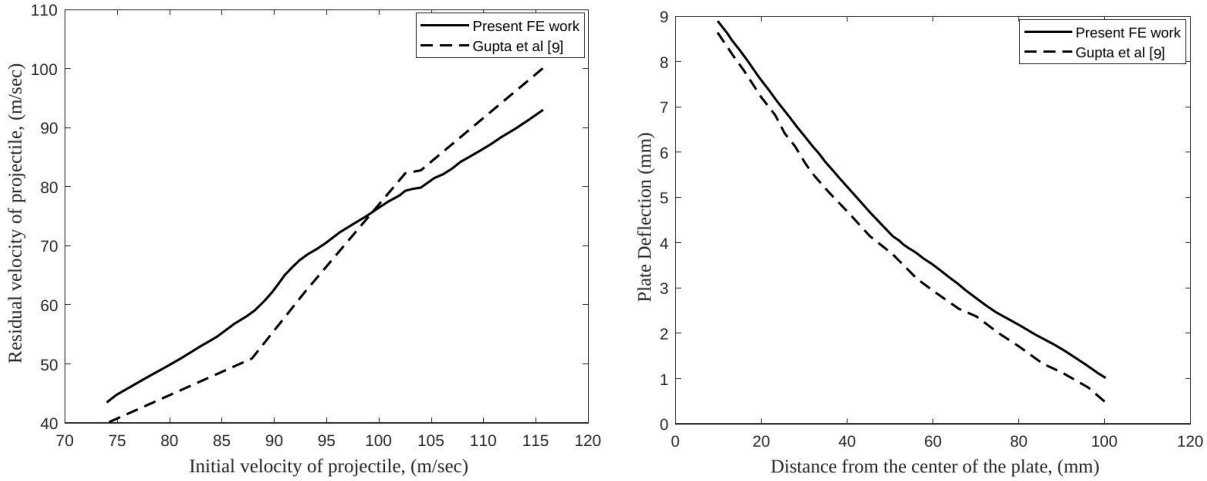

(a) Residual velocity of the projectile after impact (b) Deflection of the target body under impact

Fig. 3. Validation of the finite element formulation

The impact zone in the target body is divided into the following three zones: top (zone T), middle (zone M) and bottom (zone B), as shown in Fig. 4. Fig. 5 presents the fracture behavior of the target body at different time steps with the impact velocity of 115.6 m s^{-1}. The von Mises stress contours are used to show the maximum stress values in the target body. It is observed that due to the blunt nature of the projectile, the fracture initiates in zone B under the outer edge of the projectile due to tensile tearing. The fracture propagates from zone B to zone T of the target body resulting in the shear plug formation as the thickness of the target body is 1 mm.

3.2. Effect of prestress on the impact response

Next, the effect of prestress on the fracture behavior of the target was analyzed. Fig. 6 shows the fracture behavior at different time steps in a stress-free target body. It is observed that the fracture initiates in zone T due to tensile tearing along the outer edge of the projectile due to the higher thickness of the target body. The fracture propagates from zone T to zone B of the target body leading to shear plug formation. It was observed that in all four cases of prestress conditions, the fracture initiates at zone T under the outer edge of the projectile and propagates to zone B. Figs. 7 and 8 show the sectional and isometric views of the plug formation with contours for accumulation of damage when the target body is subjected to different prestress

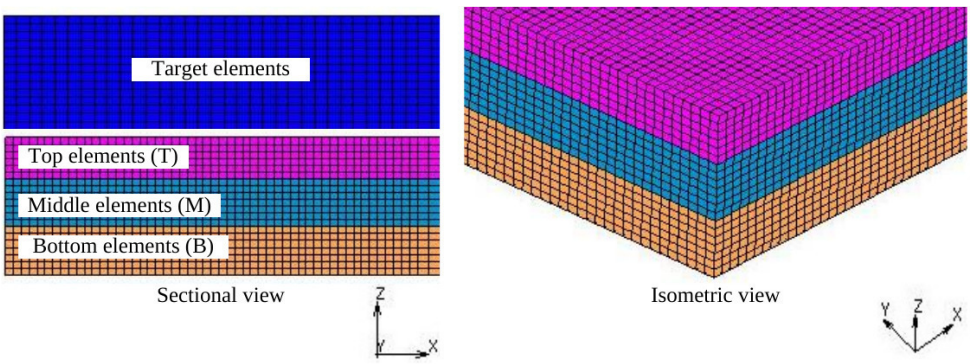

Fig. 4. Discretization of the target body into different zones

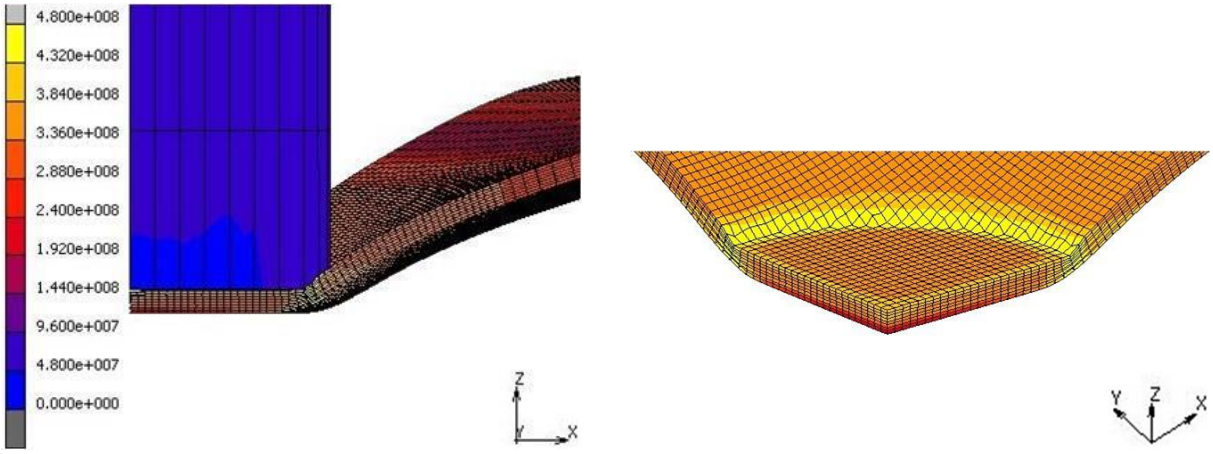

(a) At 35 μs

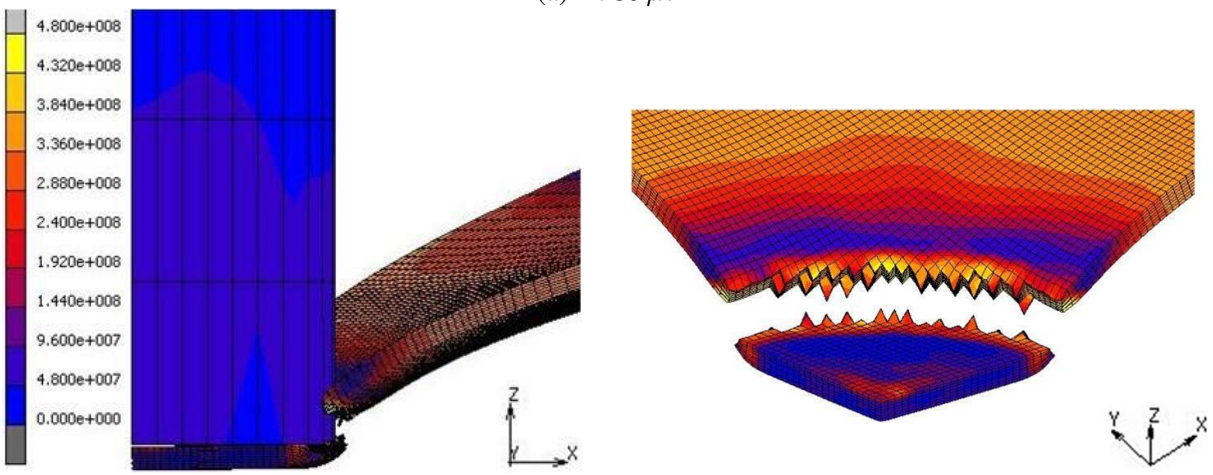

(b) At 45 μs

Fig. 5. Fracture behavior of the target body at different time steps with impact velocity of 115.6 m s^{-1} (von Mises stress [Pa])

conditions. It is found that with a stress-free state, a larger number of elements experiences a fracture in zone B in comparison to other zones, leading to fragmentation.

The material in zone T remains intact. Further, the material at the center of the plug also demonstrates fracture that may be due to oscillation of stress waves leading to cavity formation in zone M. Zone B and zone M demonstrate more fracture with compressive prestress conditions demonstrating cavity formation between zone B and zone T. A similar phenomenon has also been observed in the target body under combined loading, where the fracture is observed at zone M leading to cavity formation. The size of the cavity is a bit smaller in comparison to the compressive prestress condition. This is due to the presence of the tensile prestress in the combined loading case, which is further justified by analyzing the plug formed in the target body with the tensile prestress condition.

The presence of tensile prestress in the target body tends to arrest the fracture up to the edge of the plug. The observation is in agreement with the one made by Reddy and Mohandas [19], stating that the tensile residual stresses are beneficial for ballistic performance. The plug formation through the tensile tearing has also been delayed in the presence of the tensile prestress in the target body. The prediction has also been substantiated in the following section

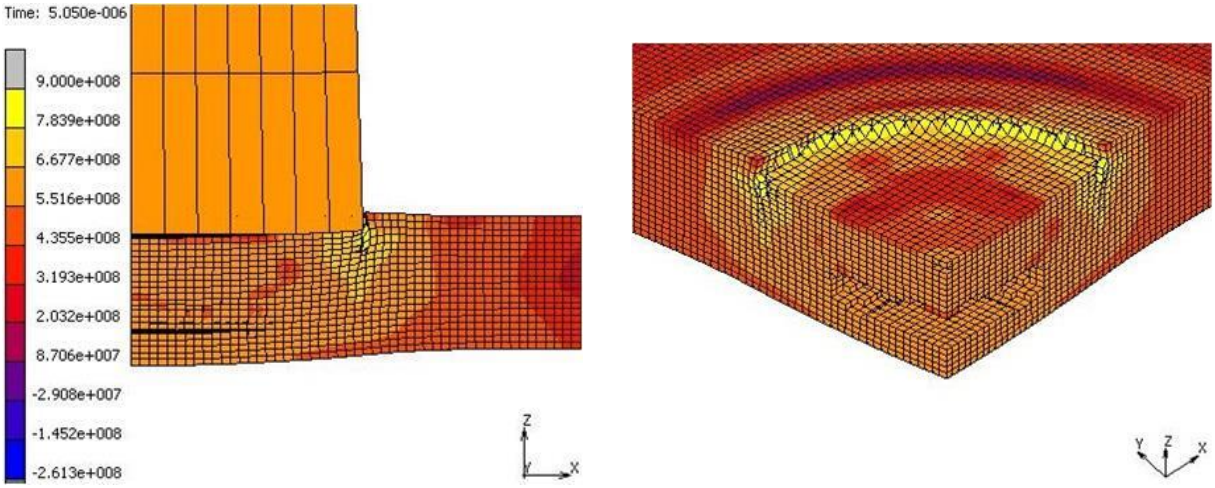

(a) At 5 μs

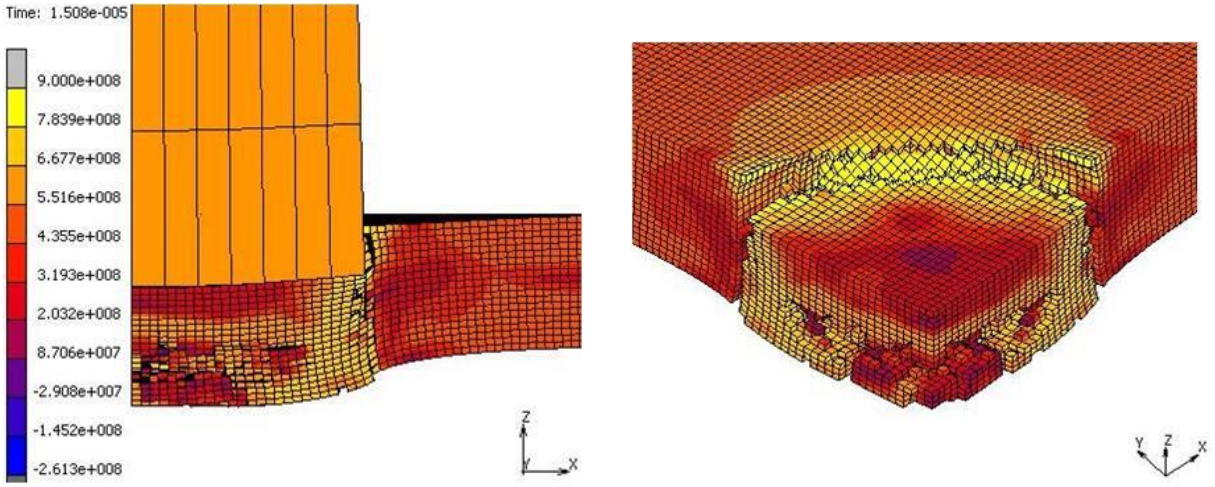

(b) At 15 μs

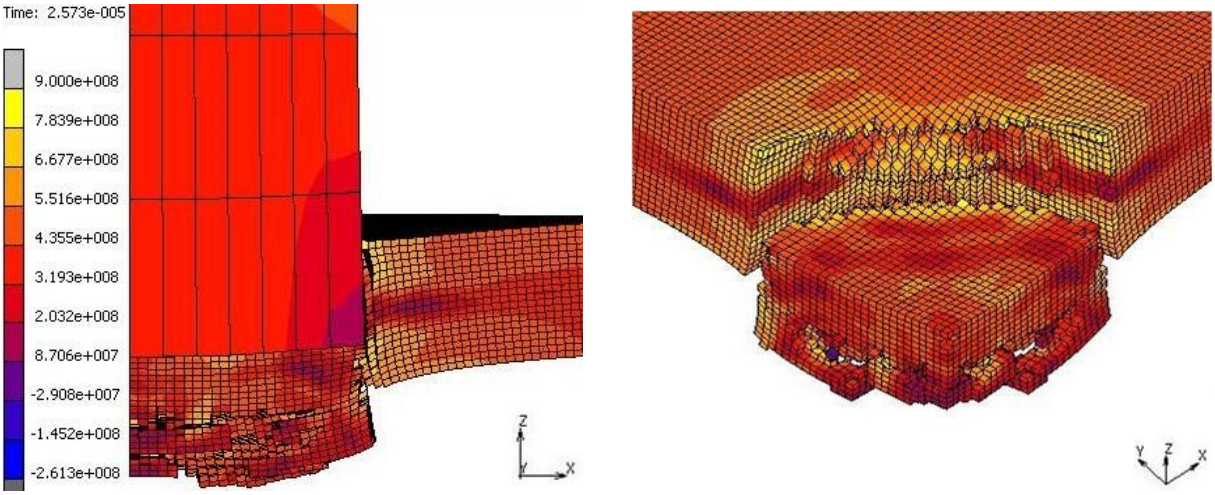

(c) At 25 μs

Fig. 6. Fracture behavior during the impact of a blunt projectile on the stress-free target body (von Mises stress [Pa])

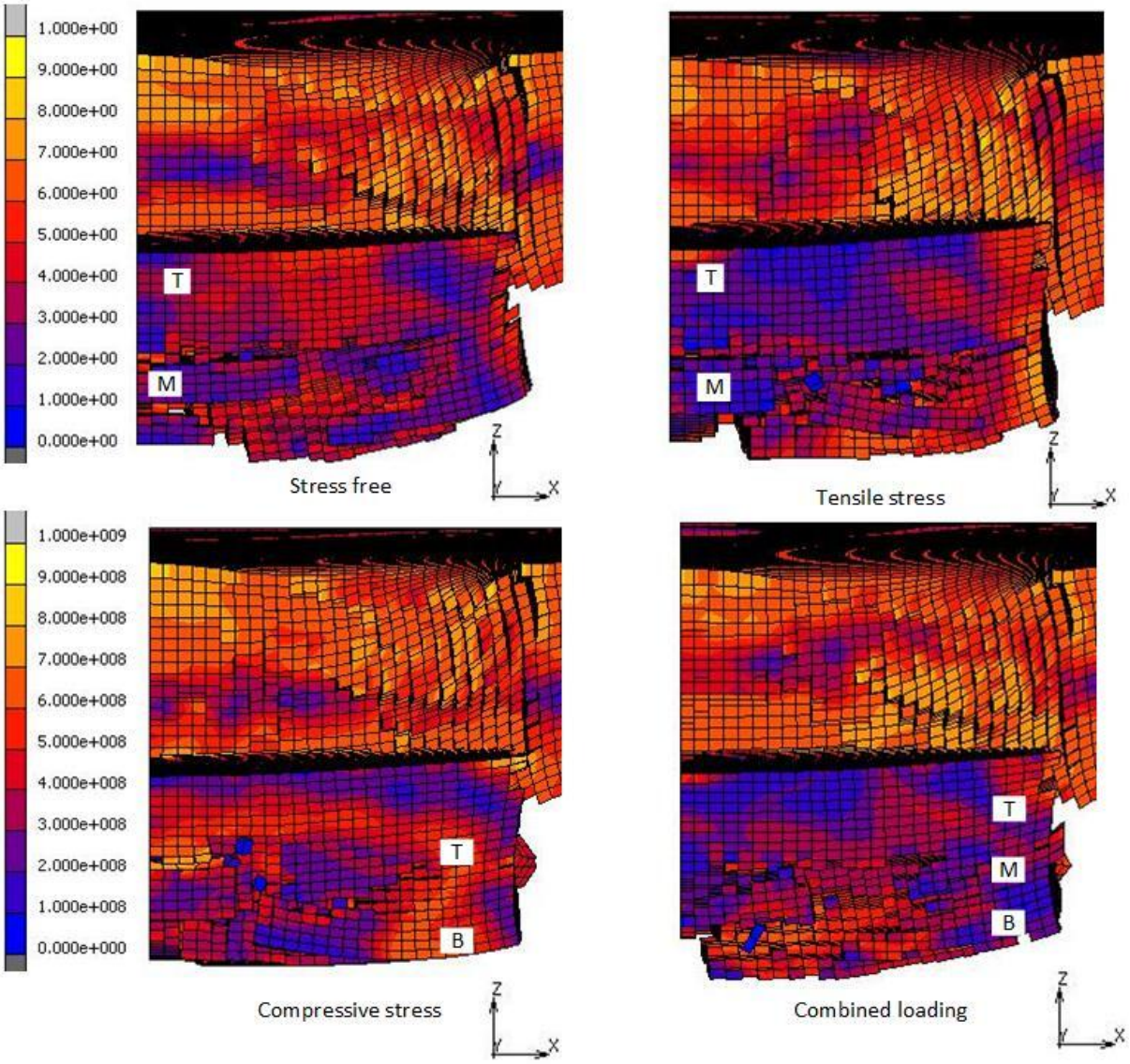

Fig. 7. Effect of prestress on the fracture behavior in the target body (sectional view) (von Mises stress [Pa])

considering the different parametric evolution in the target body. Minimum fracture is observed in the target body with tensile prestress, whereas maximum fracture is observed in the material with the compressive prestress condition. The fracture behavior of the combined loading case is like that of the compressive condition, where the presence of compressive components tends to increase the fracture.

3.3. Effect on the distribution of stress triaxiality

The fracture in a material prominently depends upon the stress triaxiality. As the target body is impacted by a projectile, the stress wave evolves and travels throughout the body. The higher magnitude of stress triaxiality with tensile nature results in fracture of the structure catastrophically; by contrast, the compressive nature of stress triaxiality does not induce any fracture. The variation of stress triaxiality is evaluated at two locations: point P (i.e., at the impacting face on the target body under the outer edge of the projectile) and point M (i.e., the geometric

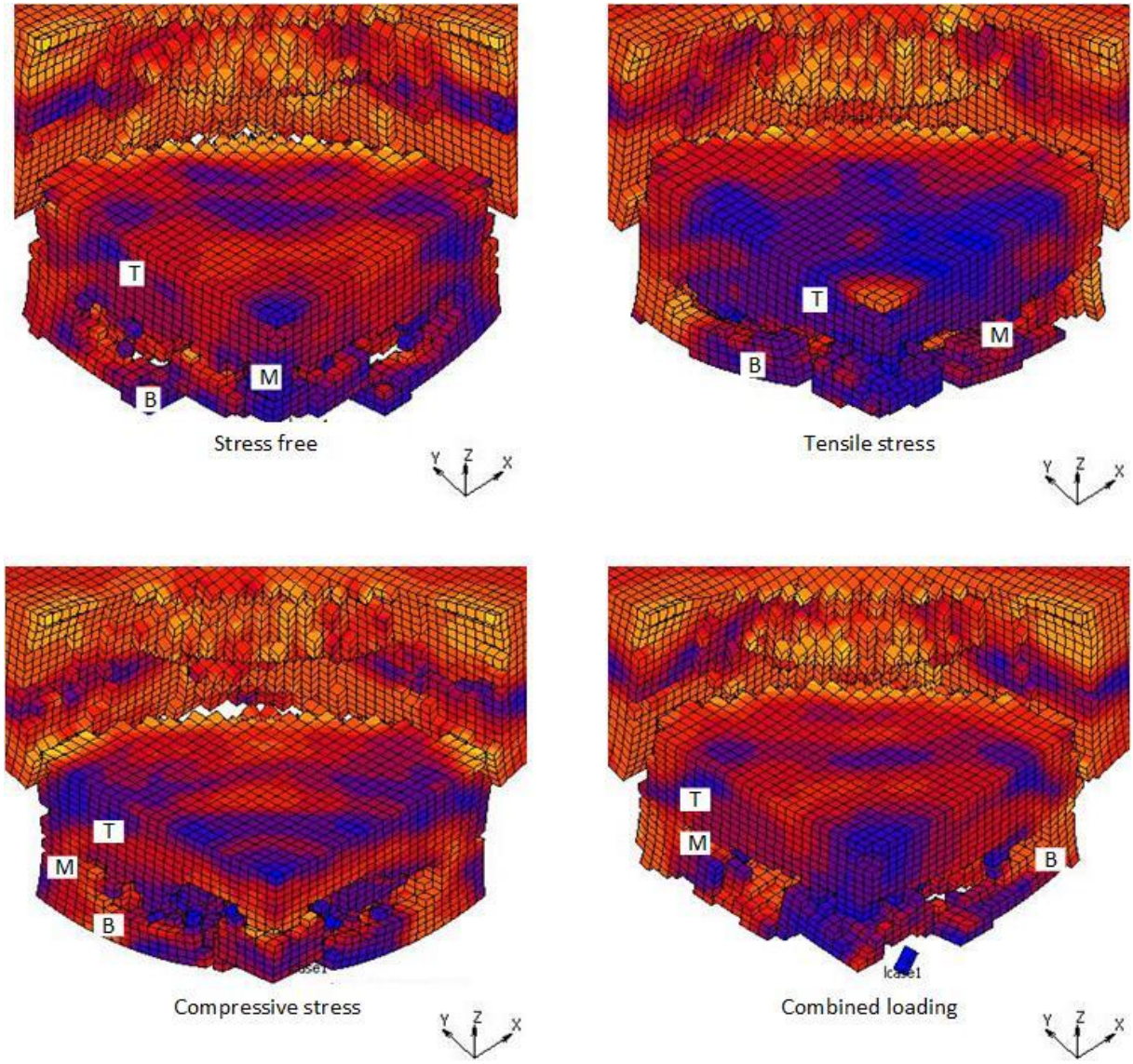

Fig. 8. Effect of prestress on the fracture behavior in the target body (isometric view) (von Mises stress [Pa])

center of the target body), see Fig. 1. Fig. 9a-b presents the stress triaxiality at points P and M, respectively. The stress triaxiality at point P remains below the cut-off value up to about $2\,\mu$s and remains above the cut-off value with tensile prestress conditions. This is due to the presence of tensile prestress present in the target body. It is observed that the stress triaxiality with tensile prestress remains below the cut-off value during the initial stages of analysis. The stress triaxiality value for stress-free and compressive prestress conditions attains the maximum value at around $6.5\,\mu$s, whereas for the other two cases, it attains the maximum value at the later stages of the analysis. The magnitude of the stress triaxiality remains lower than the cut-off value during the subsequent time steps.

The distribution of stress triaxiality on the geometric center (at point M) is different from that of point P. The maximum value of triaxiality has been observed in the target body for all the cases. There is a high fluctuation of stress triaxiality during the analysis due to the oscillation of projectile material along the central axis [7] and the presence of tensile forces at the geometric

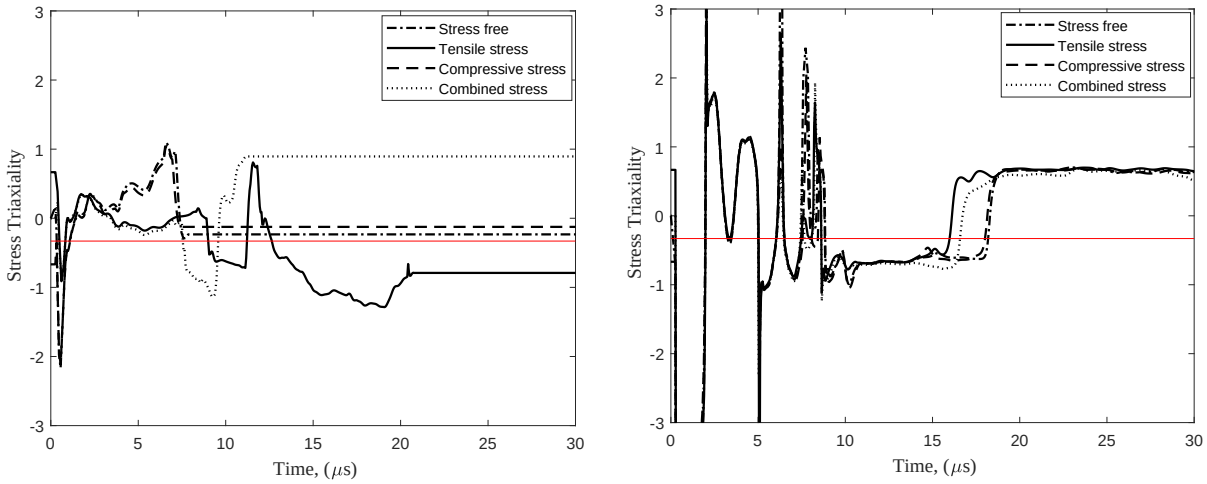

(a) At point P (b) At point M

Fig. 9. Distribution of stress triaxiality in the target body

center due to the stretching deformation of the material in the target body. Further, it is observed that the stress triaxiality at point M demonstrates larger values compared to those of point P.

3.4. Effect on the distribution of equivalent plastic strain

The effect of prestress on the equivalent plastic strain has been analyzed. The incremental equivalent plastic strain is an important parameter for determining the fracture in a body. Larger increments of equivalent plastic strain result in the accumulation of damage at a higher rate. Fig. 10 presents the effect of different prestress conditions on the equivalent plastic strain at points P and M. It is observed that the target body with stress-free and compressive prestress conditions results in the maximum equivalent plastic strain at around $5\,\mu$s; by contrast, the target body with tensile prestress and combined prestress conditions demonstrates the maximum equivalent plastic strain after about $10\,\mu$s.

The trend of equivalent plastic strain at the geometric center (at point M) of the target body shows a different trend, see Fig. 10b. It is observed that the material at point M experiences higher plastic deformation and shows a larger value of equivalent plastic strain with compressive prestress conditions. On the contrary, at the same location with tensile prestress conditions, the material shows a lower value of equivalent plastic strain in comparison to all other cases. The magnitude of deformation and values of equivalent plastic strain is found to be the same during the initial stages of analysis (i.e., up to around $3\,\mu$s) in all the cases. Later, the magnitude of plastic deformation in the target material at the same location (i.e., at point M) shows different trends due to the presence of different prestress conditions. The compressive prestress conditions induce maximum equivalent plastic strain, whereas the tensile prestress conditions result in minimum values. Further, the effect of the equivalent plastic strain is prominent in the later stages of the impact process.

3.5. Effect on the accumulation of damage

The deforming material shows fracture due to the presence of a mathematical scalar parameter termed ”damage”. The effect of prestress on the accumulation of damage in the target body has been analyzed. The damage model given in (5) has been implemented in the finite element

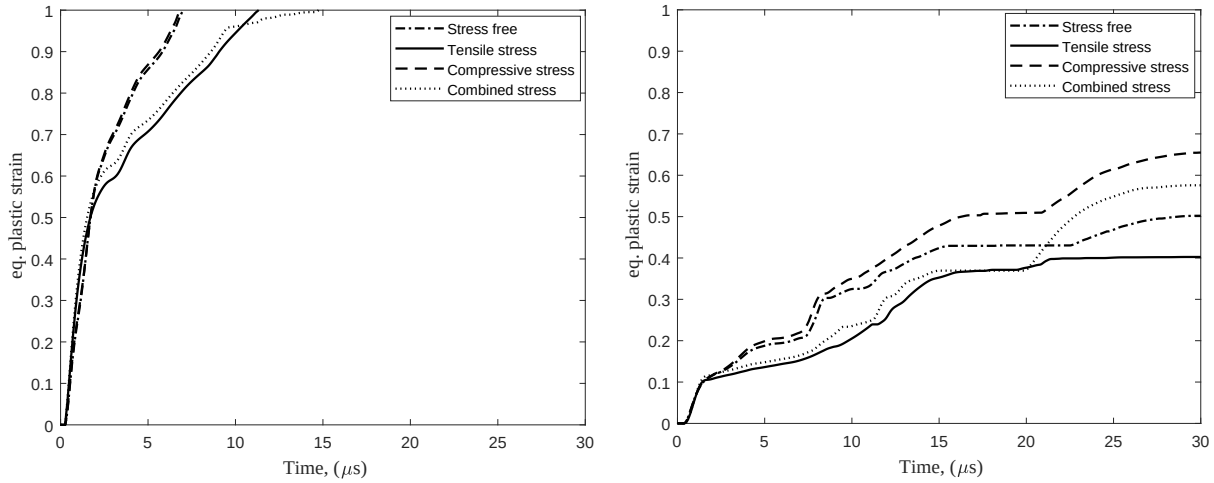

(a) At point P (b) At point M

Fig. 10. Distribution of equivalent plastic strain in the target body

formulation with the help of a Fortran-based external user subroutine. The relationship for finding the damage is given in (5). The accumulation of damage is a function of equivalent plastic strain and fracture strain. The fracture strain is dependent on the stress triaxiality as given in (6). Therefore, the accumulation of damage at any point in the problem domain can be explained with the help of the equivalent plastic strain and the stress triaxiality. In the model, the effect of "cut-off stress triaxiality" (less than $-1/3$) has also been implemented. The accumulation of damage at points P and M in the target body is presented in Fig. 11.

It is observed that due to the geometry of the problem, the accumulation of damage is different at point P and point M, as apparent from Fig. 11. At point P (Fig. 11a), the rate of accumulation of damage is very high with compressive prestress conditions, while it is minimal with tensile prestress conditions in comparison to other cases. The stress triaxiality and equivalent plastic strain values are higher with compressive prestress conditions with respect to other cases, resulting in a higher accumulation of damage, Figs. 9a and 10a. One can observe that

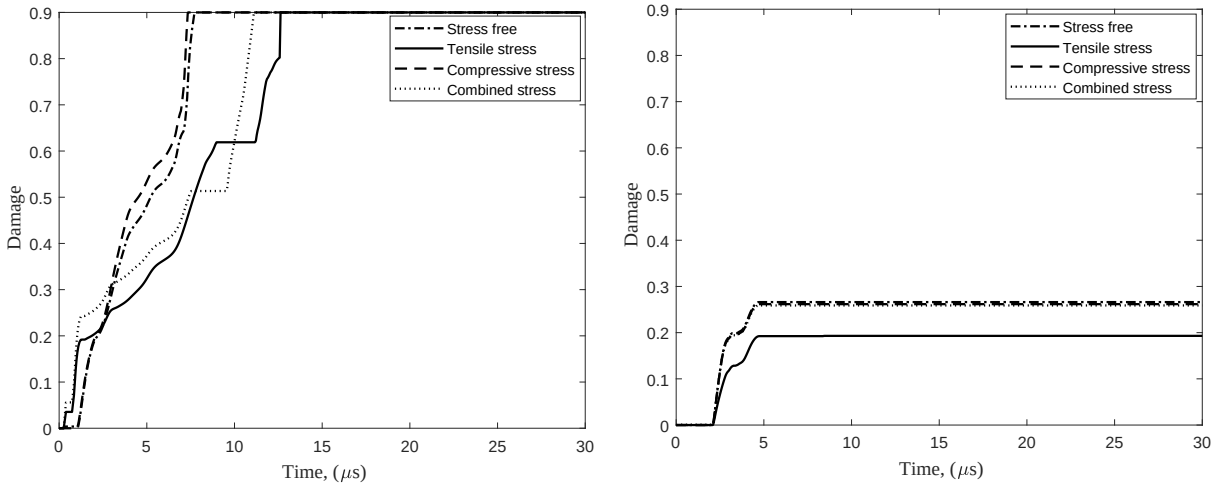

(a) At point P (b) At point M

Fig. 11. Accumulation of damage in the target body

the stress triaxiality remains positive throughout the analysis after the initial time step of around $2\,\mu$s with compressive prestress conditions, Fig. 9a. In view of these parameters, the material at point P experiences earlier fracture with compressive prestress conditions. The accumulated damage values at point P with compressive prestress and stress-free conditions reach the critical value of damage at around $6\,\mu$s, whereas the accumulated damage values with tensile prestress and combined prestress conditions reach the critical value of damage at around $10\,\mu$s, Fig. 11a. Moreover, during the initial time step up to around $2 \sim 3\,\mu$s the stress triaxiality is higher with respect to other cases, while the equivalent plastic strain values are almost the same. This results in a higher accumulation of damage during the initial time steps. But after around $2 \sim 3\,\mu$s, the rate of accumulation of damage is much higher with compressive prestress conditions compared to the cases at point P, Fig. 11a. The rate of accumulation of damage in stress-free and combined prestress conditions is in between these two cases, in line with the observations reported at point P in Figs. 9a and 10a, respectively.

The accumulation of damage at the geometric center (at point M) also follows a similar trend, as depicted in Fig. 11b. The accumulation is the same during the initial stages, but it grows with time. It is observed from Fig. 9b that there is a high fluctuation of stress triaxiality at point M but overall the values are more or less the same for all the cases. Therefore, the accumulation of damage can be explained with the help of equivalent plastic strain. The lower magnitude of equivalent plastic strain results in the lower accumulation of damage at point M. The fracture initiates at the circular periphery of the target due to a higher magnitude of equivalent plastic strain. The incremental plastic strain is minimal in the tensile prestress conditions and maximal in the compressive prestress conditions. The presence of compressive prestress results in higher values of equivalent plastic strain. Therefore, the accumulation of damage will be higher compared to the tensile prestress, where the magnitude of equivalent plastic strain is lower. It is also predicted that in the combined stress condition, the tensile prestress is more prominent compared to the compressive prestress. In view of the above observations for points P and M, one can deduce that the fracture propagates from point P of the target, while it remains constant at point M during the impact process, Fig. 11. Further, the presence of tensile prestress increases the ballistic performance of the target body as it demonstrates lower values of stress triaxiality and equivalent plastic strain.

3.6. Effect on the von Mises stress distribution

The trends for the von Mises stress with respect to time at the top, mid-plane and bottom surfaces along the thickness direction of the target plate are analyzed under high velocity impact, as shown in Fig. 12. As stated earlier, for the simplicity of the analysis, prestress has been assumed to be uniformly distributed throughout the plate enabling in-depth investigation of the fracture behavior under high velocity impact. The von Mises stress distribution, which changes during high velocity impact (Fig. 12), also illustrates this effect of uniform prestress conditions. During the initial time steps, the effect of prestress was visualized. The distribution is highly non-linear due to the complex nature of the impact. One can visualize that the presence of prestress conditions has a non-prominent effect on the trend of the von Mises stress at these intersections. The damage and stress distribution of the material under high velocity impact tends to reach its maximum value during the initial phase of the impact, while the distribution at the mid-plane and bottom surfaces of the target plate tends to fluctuate once it reaches its maximum peak. The fluctuations in the distribution are due to the force exerted by the blunt projectile that tends to push the material forming a plug.

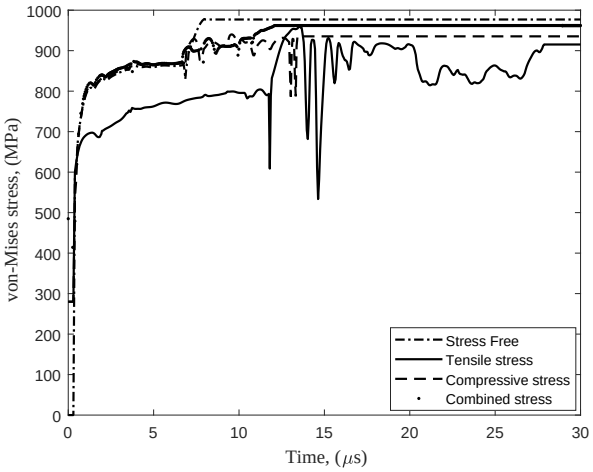

(a) At the top surface of the target plate

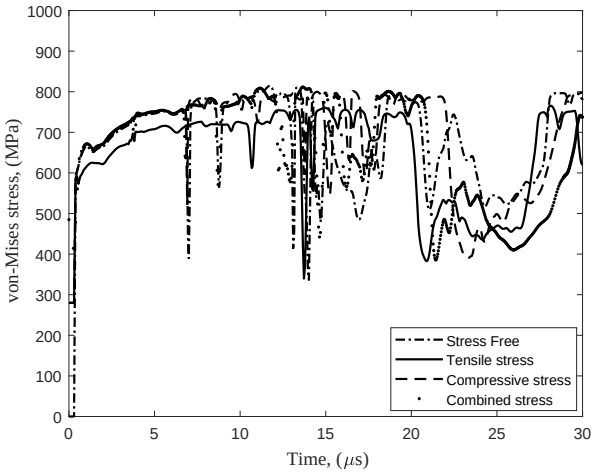

(b) At the mid-plane surface of the target plate

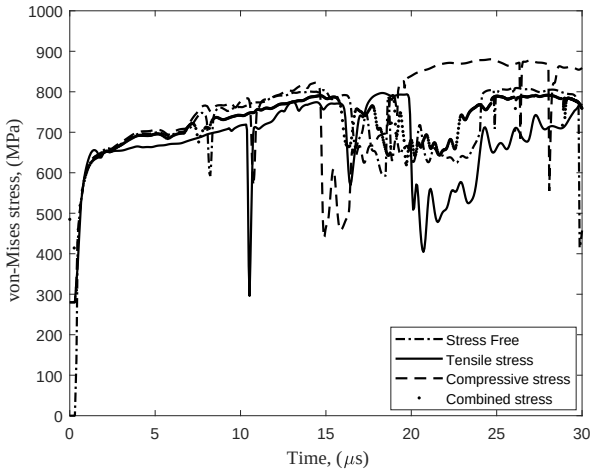

(c) At the bottom surface of the target plate

Fig. 12. Von Mises stress distribution at the top, mid-plane and bottom surfaces of the target plate

4. Conclusions

A thermo-mechanical analysis of the impact on a flat square target body was carried out for a 6 mm thick mild steel plate to analyze the effect of prestress conditions on fracture behavior. The formulation was developed to apply the prestress conditions on the target material under high velocity impact using a blunt-faced circular rigid projectile. The model was validated using stress-free conditions as no relevant literature was available. Four different conditions were simulated: stress-free target, target subjected to tensile prestress, compressive prestress, and combined bi-axial (tensile and compressive) prestress. MSC Marc Mentat^{TM} was applied for the finite element simulation. From the present study, the following conclusions were drawn:

- Different fracture behavior was observed due to the presence of prestress in the target body.
- The target material showed shear plug formation under high velocity impact with all the prestress conditions.
- The accumulation of damage accumulation in the target with tensile prestress conditions was lower compared to other conditions.

- In the combined loading condition, where the effect of both tensile and compressive prestress conditions was considered, the tensile component of prestress was dominant in comparison to the compressive prestress.

It is concluded that the tensile prestress in the target body improves the overall ballistic performance, whereas the presence of compressive prestress degrades the ballistic performance of the target body.

Acknowledgement

The support from the Council of Scientific Industrial Research (CSIR), New Delhi to carry out the present investigation in the form of a senior research fellowship is acknowledged.

References

[1] Bathe, K. J., Finite element procedures, Englewood Cliffs, New Jersey, 1996.

[2] Børvik, T., Hopperstad, O. S., Berstad, T., Langseth, M., Perforation of 12 mm thick steel plates by 20 mm diameter projectiles with flat, hemispherical, and conical noses: Part II: Numerical simulations, International Journal of Impact Engineering 27 (1) (2002) 37–64. https://doi.org/10.1016/S0734-743X(01)00035-5

[3] Børvik, T., Langseth, M., Hopperstad, O. S., Malo, K. A., Ballistic penetration of steel plates, International Journal of Impact Engineering 22 (9–10) (1999) 855–886. https://doi.org/10.1016/S0734-743X(99)00011-1

[4] Børvik, T., Langseth, M., Hopperstad, O. S., Malo, K. A., Perforation of 12 mm thick steel plates by 20 mm diameter projectiles with flat, hemispherical, and conical noses: Part I: Experimental study, International Journal of Impact Engineering 27 (1) (2002) 19–35. https://doi.org/10.1016/S0734-743X(01)00034-3

[5] Carlucci, D. E., Jacobson, S. S., Ballistics: Theory and design of guns and ammunition, CRC Press, 2008.

[6] Domun, N., Kaboglu, C., Paton, K. R., Dear, J. P., Liu, J., Blackman, B. R., Liaghat, G., Hadavinia, H., Ballistic impact behavior of glass fibre reinforced polymer composite with 1D/2D nanomodified epoxy matrices, Composites Part B: Engineering 167 (2019) 497–506. https://doi.org/10.1016/j.compositesb.2019.03.024

[7] Gautam, S., Saxena, R., A finite element study on effect of frictional heating in the Taylor rod impact problem, World Journal of Engineering 11 (6) (2015) 529–542. https://doi.org/10.1260/1708-5284.11.6.529

[8] Gautam, S. S., Saxena, R. K., A numerical study on effect of strain rate and temperature in the Taylor rod impact problem, International Journal of Structural Changes in Solids 4 (2012) 1–11.

[9] Gupta, N. K., Iqbal, M. A., Sekhon, G. S., Experimental and numerical studies on the behavior of thin aluminum plates subjected to impact by blunt- and hemispherical-nosed projectiles, International Journal of Impact Engineering 32 (12) (2006) 1921–1944. https://doi.org/10.1016/j.ijimpeng.2005.06.007

[10] Gürgen, S., Impact behavior of preloaded aluminum plates at oblique conditions, Arabian Journal for Science and Engineering 44 (2019) 1649–1956. https://doi.org/10.1007/s13369-018-3636-x

[11] Gürgen, S., Kuşhan, M. C., The ballistic performance of aramid-based fabrics impregnated with multi-phase shear thickening fluids, Polymer Testing 64 (2017) 296–306. https://doi.org/10.1016/j.polymertesting.2017.11.003

[12] Iqbal, M. A., Senthil, K., Bhargava, P., Gupta, N. K., The characterization and ballistic evaluation of mild steel, International Journal of Impact Engineering 78 (2015) 98–113. https://doi.org/10.1016/j.ijimpeng.2014.12.006

[13] Jasra, Y., Kumar, P., Ojha, N. K., Saxena R. K., Comparative study to analyze deformation/fracture behavior under high velocity impact using different dynamic transient operators, Proceedings of the 12th International Conference on Computational Methods (ICCM-2021), Vietnam, Ho Chi Minh City University of Technology, 2021, pp. 1–15.

[14] Jasra, Y., Singhal, S., Saxena, R. K., Effect of joint design on residual stresses in AISI-304 stainless steel weldment – a numerical study, Journal of Mechanical Science and Technology 35 (2021) 2167–2176. https://doi.org/10.1007/s12206-021-0433-3

[15] Lemaitre, J., Desmorat, R., Engineering damage mechanics: Ductile, creep, fatigue and brittle failures, Springer Science & Business Media, 2006.

[16] Mohammad, Z., Gupta, P. K., Baqi, A., Experimental and numerical investigations on the behavior of thin metallic plate targets subjected to ballistic impact, International Journal of Impact Engineering 146 (2020) 1–20. https://doi.org/10.1016/j.ijimpeng.2020.103717

[17] Raguraman, M., Deb, A., Gupta, N. K., CAE-based prediction of projectile residual velocity for impact on single and multi-layered metallic armour plates, Latin American Journal of Solids and Structures 6 (3) (2009) 247–263.

[18] Rathore, K. K., Jasra, Y., Saxena, R. K., Numerical simulation of fracture behavior under high velocity impact for Aluminium alloy 6060 target plate, Materials Today: Proceedings 28 (3) (2020) 1809–1815. https://doi.org/10.1016/j.matpr.2020.05.214

[19] Reddy, G. M., Mohandas, T., Influence of welding process and residual stress on ballistic performance, Journal of Material Science Letters 15 (1996) 1633–1635. https://doi.org/10.1007/BF00278111

[20] Saleh, M., Luzin, V., Kariem, M. A., Thorogood, K., Ruan, D., Experimental measurements of residual stress in ARMOX 500T and evaluation of the resultant ballistic performance, Journal of Dynamic Behavior of Materials 6 (2020) 78–95. https://doi.org/10.1007/s40870-019-00231-w

[21] Teng, X., Wierzbicki, T., Hiermaier, S., Rohr, I., Numerical prediction of fracture in the Taylor test, International Journal of Solids and Structures 42 (9–10) (2005) 2929–2948. https://doi.org/10.1016/j.ijsolstr.2004.09.039

[22] Yadav, S., Singhal, S., Jasra, Y., Saxena, R. K., Determination of Johnson-Cook material model for weldment of mild steel, Materials Today: Proceedings 28 (3) (2020) 1801–1808. https://doi.org/10.1016/j.matpr.2020.05.213